



Photosensitivity and Photocatalytic Activity of ZnO Thin Films Annealed in Different Environmental Conditions

Deepu Thomas¹ · K. E. Rakesh² · Kishor Kumar Sadasivuni³ · Jibish Mathew⁴ · Joshy Joseph¹ · Kalim Deshmukh⁵

Received: 30 October 2021 / Accepted: 13 April 2022 / Published online: 10 May 2022
© The Minerals, Metals & Materials Society 2022

Abstract

The microwave-assisted successive ionic layer adsorption and reaction (mSILAR) deposition method was employed for the synthesis of nano-polycrystalline zinc oxide (ZnO) thin film. In this study, annealing of the prepared ZnO samples was carried out in an air and argon atmosphere. The morphology, crystallinity, and phase of the deposited nanostructured ZnO films were established with a field-emission scanning electron microscope (FESEM) and x-ray diffraction (XRD), respectively. The elemental compositions and chemical states of the ZnO nanostructures were determined by x-ray photoelectron spectroscopy (XPS), and the surface properties were evaluated using Brunauer–Emmett–Teller (BET) surface area analysis. The semiconducting behavior of the film was examined by plotting the current–voltage (I – V) characteristics. Moreover, temperature-dependent electrical resistance, photoconductivity, and photocatalytic studies were also carried out. This study showed that by electron beam irradiation, the electrical and photocatalytic activity, and the photo-conducting properties of ZnO thin film can be improved to the desired level.

Keywords mSILAR · zinc oxide · irradiation · photosensor · photocatalyst

Introduction

Semiconducting nanomaterials play a vital role in the development of a wide range of photocatalytic materials.^{1–3} Among various semiconductor metal oxides, zinc oxide (ZnO) has emerged as a subject of intensive study. ZnO is a II–VI group material with a hexagonal wurtzite structure, which exhibits inherently n -type semiconductor behavior. Moreover, due to high transparency in the visible

region, tunable electrical properties, biocompatible nature, exceptional optical property, hardness, and wide band gap of ~ 3.37 eV, ZnO is extensively used in photonics and optoelectronics, and in electromechanical, electrochemical, and biological applications.^{4–11} ZnO is the appropriate material for the fabrication of light-emitting diodes, piezoelectric transducers, laser/nanolaser diodes, gas sensors, UV sensors, varistors, and spintronics.^{12–19} ZnO thin films can also be used as transparent conducting windows in solar cell devices.^{20–22} Infrared reflectance, visible transmittance, and improved electrical properties can be achieved by slight modifications in ZnO.^{18–20} Presently, many different techniques have been applied for the synthesis of visibly transparent as well as conducting thin films of ZnO. For example, ZnO thin films are being prepared by a number of different methods, such as chemical bath deposition,²³ electrodeposition,²⁴ sol–gel process,^{25–31} pulsed laser deposition,^{32–37} ball mixing method,³⁸ metal oxide chemical vapor deposition,³⁹ seed-mediated growth,⁴⁰ atomic layer deposition,⁴¹ chemical vapor deposition,^{42–44} successive ionic layer adsorption and reaction (SILAR),^{45–47} and spray pyrolysis^{48–50} etc.

Physical deposition processes have been extensively applied in thin-film technology; however, a wet synthesis process such as SILAR is low-cost, simple, and which gives

✉ Deepu Thomas
deepuskariankal@gmail.com

✉ Kalim Deshmukh
deshmukh.kalim@gmail.com

¹ Department of Physics, Nirmalagiri College,
Nirmalagiri 670701, India

² Department of Chemistry, Nirmalagiri College,
Nirmalagiri 670701, India

³ Center for Advanced Materials, Qatar University, 2713 Doha,
Qatar

⁴ Department of Electronics, Prajyoti Niketan College,
Pudukad 686301, India

⁵ New Technologies-Research Centre, University of West
Bohemia, 30100 Pilsen, Czech Republic

control at the nano-level. SILAR is economical while considering the benefits of film properties, such as controlled deposition rates, large surface area deposition, and less wastage of chemicals. During thin-film deposition by the SILAR method, a film of metal ions generated through the precursor solution is adsorbed on the substrate surface in the form of unit layers. The deposition of thin film by the SILAR method mainly involves two steps: (1) complex ion layer adsorption on the substrate surface, and (2) adsorbed ion layer reaction.⁵¹ The precipitation reaction is vital in the formation of a single layer by the reaction between the counter ion and the adsorbed ion. The pH of the reacting solutions and their concentration and precipitation reaction are of utmost importance. The SILAR method is widely accepted for the synthesis of epitaxial multilayered thin films, preferably chalcogenide (e.g., ZnSe, ZnS, CdS).⁵¹ However, certain shortcomings have been observed in the synthesis of oxide films. The thin-film deposition of ZnO by the SILAR method utilizes a multiple times chemical-dipping approach. It uses the complexes of zinc, such as zinc chloride, ammonium zincate, and sodium zincate.^{52–56} In addition, the substrate temperature and different partial pressure of oxygen affects the optical, electrical, and structural properties of the synthesized films. Furthermore, annealing will improve the quality of the thin film, while post-annealing treatment of synthesized films will help in overcoming the drawback of the SILAR method. Annealing can be carried out in different conditions, like in nitrogen, hydrogen, oxygen, or air.⁵⁷

In the present work, microwave-assisted successive ionic layer adsorption and reaction (mSILAR) was employed for the synthesis of ZnO thin films.¹⁰ The optical and photocatalytic property of the as-prepared ZnO film has been studied with respect to different annealing atmospheres. To alter the electrical conductivity, the samples were irradiated with an electron beam, and the optical response was analyzed in the presence of ultraviolet (UV) illumination. The photocatalytic response of the samples was studied by a degradation test performed on methylene blue (MB) dye.

Materials and Methods

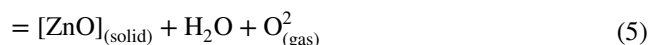
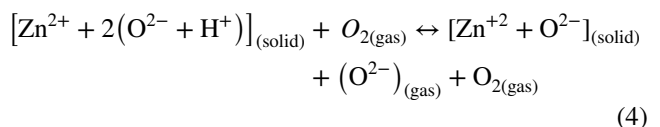
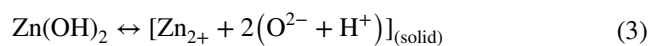
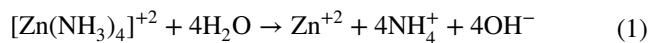
Experiment

Ammonia solution (NH₄OH), sodium hydroxide (NaOH) pellets and zinc sulfate heptahydrate (ZnSO₄·7H₂O) (all from Merck) were used without further purification. Ultrapure double-distilled water was used in the experiments.

Synthesis of Zinc Oxide

ZnO thin films were synthesized using the mSILAR technique, in which the substrate was dipped into

a ZnSO₄·7H₂O and ammonia solution, where Zn²⁺ along with NH₄OH formed a zinc ammonia complex [Zn(NH₃)₄]²⁺. During the initial stage of deposition, zinc ammonia was adsorbed onto the substrate. Afterward, with the immersion of this substrate in distilled water, the adsorbed zinc ammonia complex changes into zinc hydroxide (Zn(OH)₂). The immersion time was 30 s and the experiment was repeated 100 times. The chemical reactions involved in the growth of ZnO by the mSILAR method are as follows:



Finally, the prepared ZnO films were annealed at 450°C for 30 min in both air and an inert (argon) atmosphere.

Sensor Fabrication

The ZnO thin films were coated on an FR-4 sheet of 1.6 mm thickness using the mSILAR technique to form a sensor for measuring the effect of photosensitivity (Fig. 1). FR-4 is a composite material that consists of glass fabric and electrical grade epoxy resin. The terminals of the sensor were soldered on either side of the sheet.

Characterization of Grown Films

A Bruker AXS-8 XRD was used for the structural studies. Scanning electron microscopy (SEM; JEOL-JSM 6490

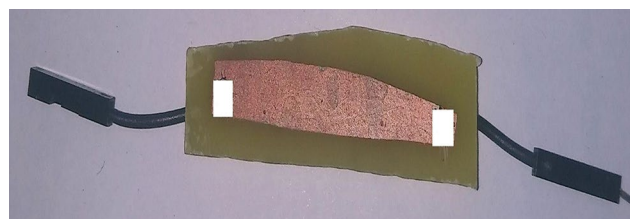


Fig. 1 The fabricated sensor used to measure the effect of photosensitivity of ZnO.

analyzer) was employed for the morphological studies. The electrical resistance of the samples was measured using a digital multimeter (Keithley 2100). An electron beam of 8 MeV energy and 8 kGy/min dose rate (Fricke dosimetry) obtained from Microtron, was used for the irradiation of the ZnO films. A Novawin 3000e Surface Area and Pore Size Analyzer were used for the Brunauer–Emmett–Teller (BET) analysis. Transmission electron micrographs (TEM) were taken using a JEOL JEM-3010.

Photoresponse and Photocatalytic Activity of ZnO Film

The photoconductivity of the ZnO films was analyzed at a wavelength of 365 nm and 1.4 mW/cm² power density using a Keithley 6485 picoammeter. The photocatalytic degradation studies were performed using a photocatalytic reactor, as depicted in Fig. 2a. For the photocatalytic degradation studies, a stock solution of MB in water was prepared in the range of 10–50 mg/L, and the grown ZnO film was placed inside 50-ml solutions in various MB concentrations. Initially, the reaction mixture was stirred in the dark to avoid the influence of adsorption by the ZnO films. Thereafter, the dye solution containing the ZnO film was irradiated with a UV light of 365 nm. The degradation by the ZnO film under UV illumination was indicated by the decolorization of the dye. Figure 2b shows the photodegradation process of MB by the ZnO film. MB is a blue-colored cationic dye that shows an absorption maximum of 664 nm. The photodegradation of MB can be seen from the decolorization of the blue color, and the extent of degradation was quantitatively measured using a UV-Vis spectrophotometer. The degradation

percentage of MB was determined spectrophotometrically at λ_{\max} 664 nm using the equation:

$$\text{MB degradation efficiency (\%)} = (C_0 - C_t) \times 100 / C_0 \quad (6)$$

where C_0 and C_t represent the initial and final concentrations, respectively, of the MB dye solution. The influence of various parameters, like contact time, initial concentration of the dye, and the reusability of catalyst, was studied.

Results and Discussion

Structural Characterization

Figure 3 shows the SEM images and XRD plots of the ZnO film annealed in air and in an argon atmosphere. The SEM analysis reveals a nano-structured flower-like growth of the ZnO by the mSILAR process. For the ZnO film annealed in the argon atmosphere, a vertically grown nanoflower-like morphology was observed, as shown in Fig. 3a. A similar morphological evolution was seen for the ZnO films annealed in air (see inset of Fig. 3a). In both samples, a uniform, vertical and dense growth of nanoflowers was noticed all over the substrate. To study the growth structure phase, crystallinity, and the effect of annealing in different environments, XRD analysis was performed. Figure 3b depicts the XRD plot of the synthesized ZnO film annealed in the inert environment and in air (Fig. 3b, inset). The ZnO film exhibited a polycrystalline nature with a hexagonal wurtzite structure, as evident from the XRD patterns. The peaks appearing at 31°, 36°, 47°, and 56° are linked, respectively, with the (100), (101), (110) and (102) reflections (JCPDS

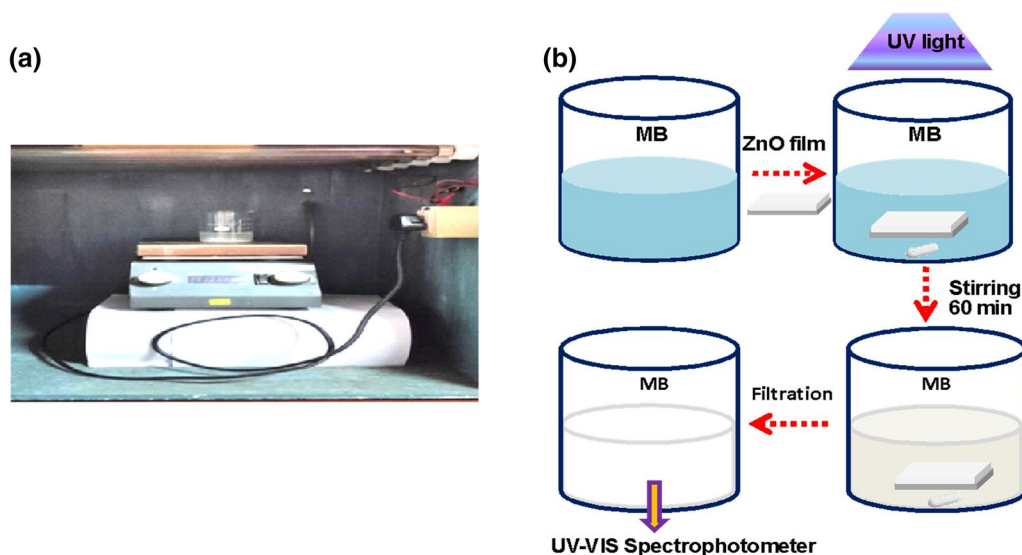


Fig. 2 Photodegradation of MB dye: (a) photodegradation chamber, (b) schematic of the photodegradation of MB dye by ZnO film.

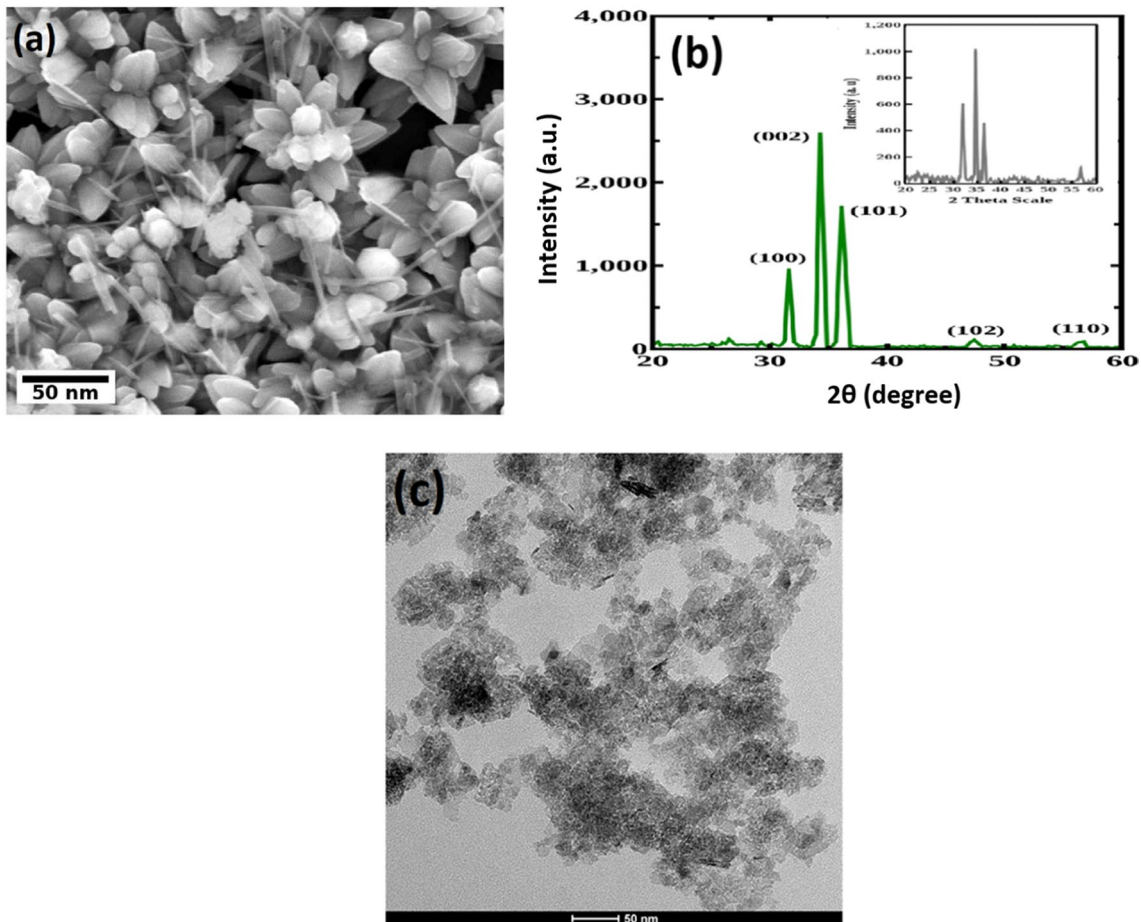


Fig. 3 (a) SEM image of ZnO film annealed in an inert environment, (b) powder XRD patterns of ZnO films annealed in an inert environment and in air (inset), (c) typical TEM image of ZnO thin film.

no. 36-1451). This confirms the wurtzite hexagonal structure of ZnO.^{58–60} In the figure, it can be seen that the peak (002) occurring at $2\theta \approx 34^\circ$ has the maximum intensity, which suggests the preferential growth of the ZnO nanostructure along the *c*-axis. The crystal grain sizes calculated using Scherrer's equation for the sample annealed in air and argon were 15.9 nm and 25.1 nm, respectively. Thus, the increased grain size and peak intensity (see Fig. 3b) of the ZnO film annealed in an inert atmosphere suggest an improved crystalline structure compared to the air-annealed ZnO films. Figure 3c depicts a TEM image of a typical ZnO thin film. The shape, size, and hexagonal crystal structure of the deposited films were confirmed by TEM. The particle sizes calculated using the Debye–Scherrer's equation was 16 nm.

The elemental compositions and chemical states of the ZnO samples were determined by XPS. The survey scan spectra (Fig. 4a) show obvious peaks for zinc and oxygen, and suggest that there are no impurities in the ZnO samples. Figure 4b presents the high-resolution Zn 2p XPS spectrum of the ZnO sample. Pure ZnO exhibited symmetrical peaks at 444.09 and 467.09 eV, due to the orbital coupling of Zn

(2p_{1/2}) and Zn (2p_{3/2}), respectively. The split peaks with a binding energy difference of 23 eV signify the strength of the spin–orbit coupling process. The typical O 1s spectra (Fig. 4c) show one peak centered at 958.39 eV. Based on the variation in charge transfer from Zn²⁺ to O²⁻ that is caused by the vacancies, the binding energies vary from the above stoichiometric values.

Surface Properties

Figure 5 depicts the adsorption–desorption isotherms for ZnO films (a) annealed in the air (unirradiated), (b) annealed in air (irradiated), (c) annealed in air argon atmosphere (unirradiated), and (d) annealed in air argon atmosphere (irradiated). According to the IUPAC classification, all the isotherms correspond to Type IV. Furthermore, their hysteresis loops are Type H₃, indicating that they are made of mesoporous materials. The absorption of the irradiated argon-annealed ZnO exhibits a gradual increase in volume adsorbed from the low relative pressure. The BET surface area of samples (a), (b), (c), and (d) was 10.7 m²/g, 10.9

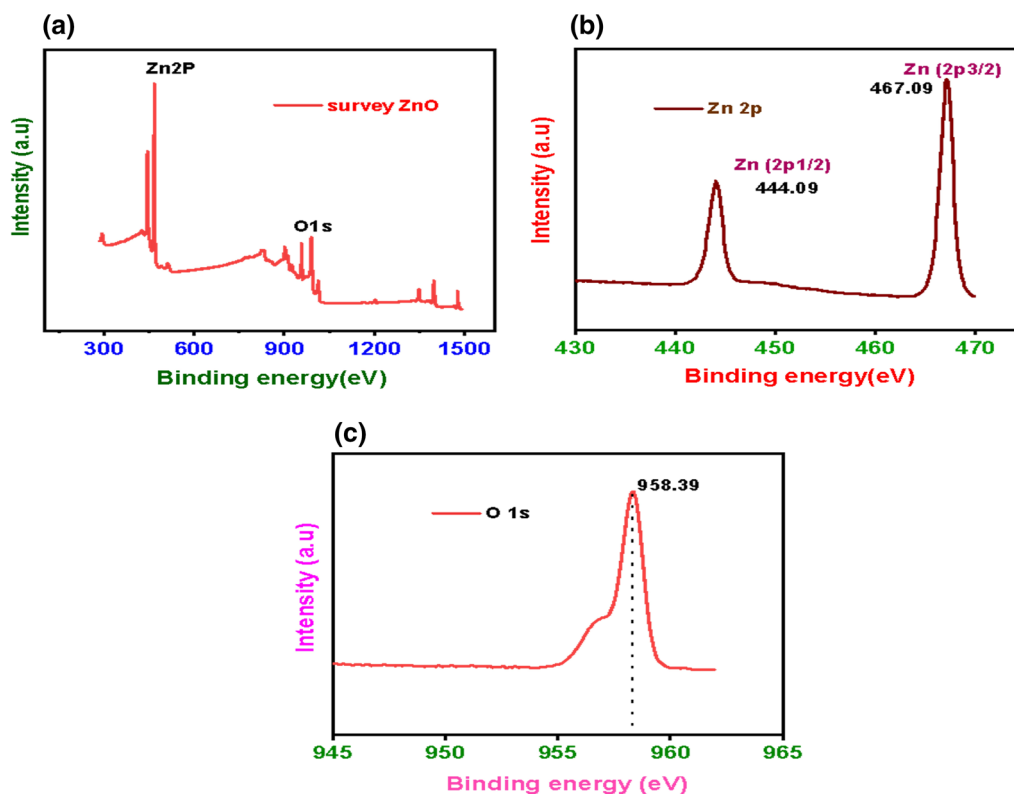


Fig. 4 (a) XPS spectra of the ZnO sample, (b) Zn2p spectrum of ZnO, and (c) O1s spectrum of ZnO.

m^2/g , $11.1 \text{ m}^2/\text{g}$, and $11.3 \text{ m}^2/\text{g}$, respectively. It can be seen that the unirradiated samples have a lower surface area than the irradiated sample. This argon-annealed (irradiated) sample possesses more surface area than the air-annealed (irradiated) sample. Figure 6 illustrates the pore size distribution of the samples, which shows that the nanoparticles were well-dispersed in the range of 15–25 nm.

Current–Voltage Characteristics and Temperature Dependency

The semiconducting properties of ZnO films annealed in air and argon atmospheres were studied by analyzing their current–voltage (I – V) characteristics. Figure 7 shows the I – V characteristics and temperature-dependent change in resistance of ZnO films before and after irradiating with an electron beam of 8 kGy, respectively. From Fig. 7a, it can be observed that all the films exhibited typical semiconductor characteristics both before and after irradiation. Compared to ZnO film annealed in air, the films annealed in an inert atmosphere show increased conductivity, and the difference is more prominent at a higher applied bias ($> \pm 5 \text{ V}$). The consequence of electron beam radiation on the I – V characteristics of thin films was studied and is depicted in Fig. 7a. I – V studies of irradiated ZnO_{air} film embraced a comparable drift in conductivity with respect to the unirradiated ZnO_{air}

film, and the current is slightly amplified in the case of the irradiated ones. A similar trend of increase in conductivity after irradiation was observed for ZnO film annealed in an inert atmosphere. I – V analysis of the film revealed that the irradiated and inert atmosphere-annealed ZnO film show higher conductivity compared to other samples. Figure 7b shows the temperature-dependent change in the resistance of air- and inert atmosphere-annealed ZnO thin films both before and after electron beam irradiation. The temperature sensing was implemented at different temperatures for all the samples. As the temperature increased from 25°C to 200°C , a significant change in the relative resistance was observed for all the samples. The relative resistance (A_R) was calculated using the equation:^{38,41}

$$A_R = \frac{R_0 - R}{R_0} \times 100 \quad (7)$$

where R_0 is the initial electrical resistance and R is the resistance in the presence of increased temperature of the material. The inert-annealed ZnO thin film exhibited an increment in the conductivity against the non-inert annealed samples. The samples were irradiated with a high-energy electron beam during the experiment. Even though Fig. 7b shows a similar trend for both the irradiated and unirradiated

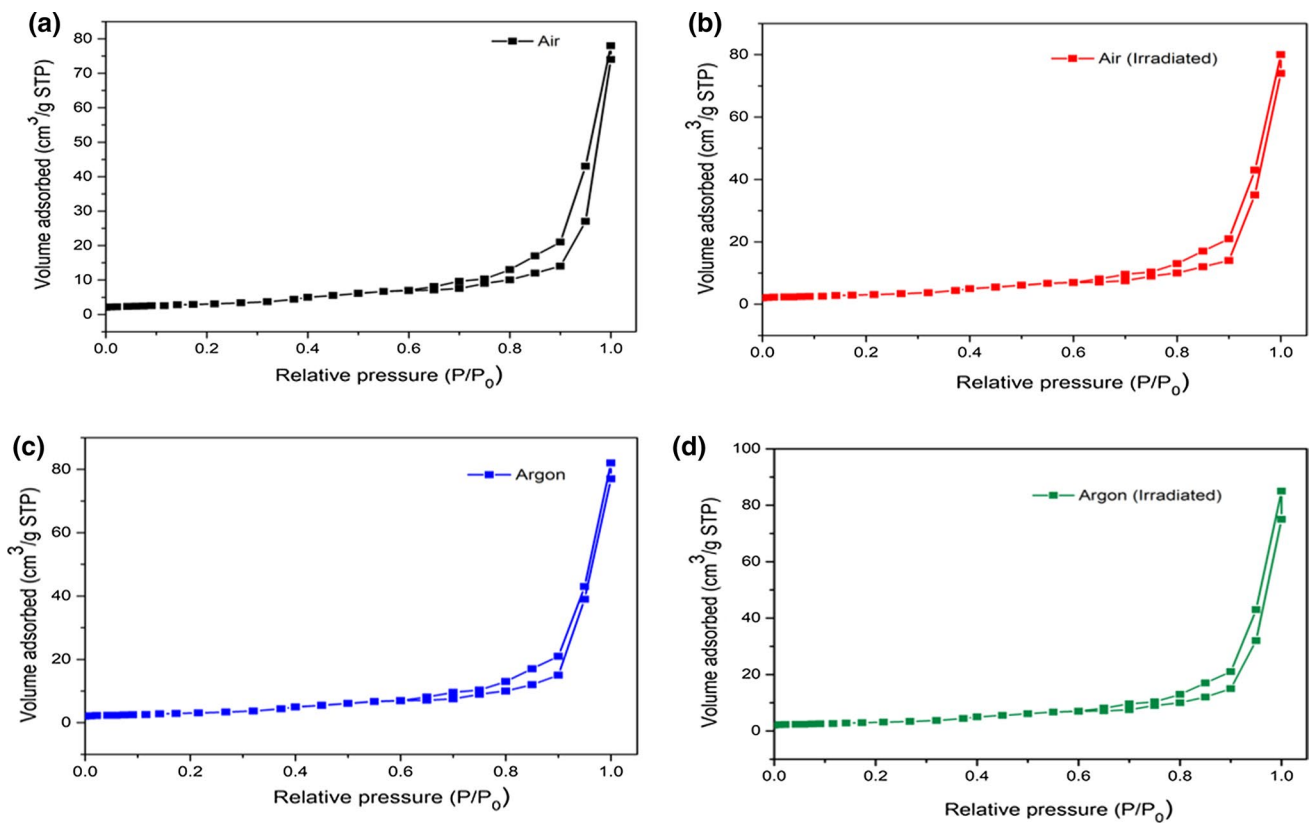


Fig. 5 Nitrogen adsorption–desorption isotherms of the ZnO nanostructures synthesized in different conditions: (a) annealed in air (unirradiated), (b) annealed in air (irradiated), (c) annealed in air

argon atmosphere (unirradiated), and (d) annealed in air argon atmosphere (irradiated).

samples, the sensing features of the irradiated one possess good results in comparison with the unirradiated samples.

Photoconductivity under UV Illumination

Figure 8a shows the photoconductivity studies of ZnO thin films annealed in air and inert atmospheres along with virgin and irradiated films. To conduct the measurements, electrodes were made on the samples by depositing gold using the thermal evaporation technique.⁶¹ The photoresponse of ZnO corresponds to the desorption and absorption of oxygen on the surface of ZnO. In the dark, oxygen molecules are absorbed on the surface by taking a free electron, and, under UV illumination, the photogenerated holes neutralize the oxygen ions and oxygen is desorbed from the surface of the ZnO. The photoconductivity of the samples was noted to be directly proportional to the applied field. The sample shows positive conductivity as the photocurrent exceeds the dark current. The photoconductivity of the inert samples was improved significantly compared with the sample annealed in a non-inert atmosphere. It is evident that the surface roughening and thickness of the films help in the charge transportation

when exposed to light.^{10,54} It was demonstrated that the photoconductivity of ZnO film will depend on the annealing condition as well as on the irradiation level. The samples were illuminated with UV at 365 nm, and the sensing properties were studied with respect to the change in resistance, as shown in Fig. 8b. The resistance of the samples (inert and non-inert) was observed to be reduced with UV illumination. The highest value of relative resistance for both the samples was observed at 13.5 h. The ZnO films initial resistances for the four samples were observed to be 99.17 kΩ, 98.76 kΩ, 94.15 kΩ, and 93.78 kΩ. The resistance of the argon-irradiated sample returned to its initial value in 45 s when the UV light was turned off, but the recovery time for the sample annealed in air-irradiated was a little higher. It was noted that all the other samples showed a similar trend in the recovery time, but the recovery time of the argon-irradiated sample was high. The variation of relative resistance opens up the scope to regulate the relative resistance to the desired value by annealing in different atmospheres and electron beam irradiation. It was observed that the differential resistance acquires an almost identical pattern; however, the relative resistance of the irradiated samples was comparably low.

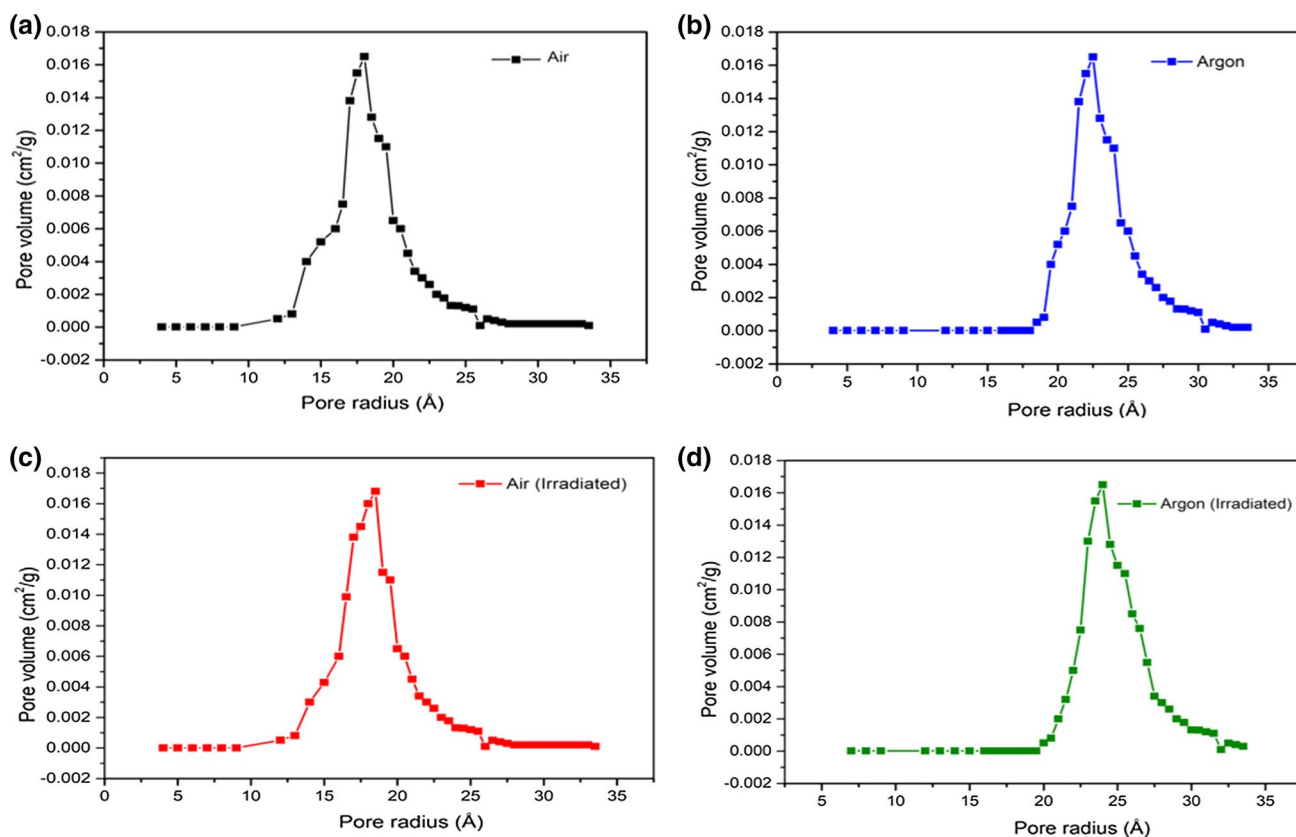


Fig. 6 Barrett–Joyner–Halenda pore size distribution curve of ZnO thin film synthesized in different conditions: (a) annealed in air (unirradiated), (b) annealed in argon atmosphere (unirradiated), (c) annealed in air (irradiated), (d) annealed in air argon atmosphere (irradiated).

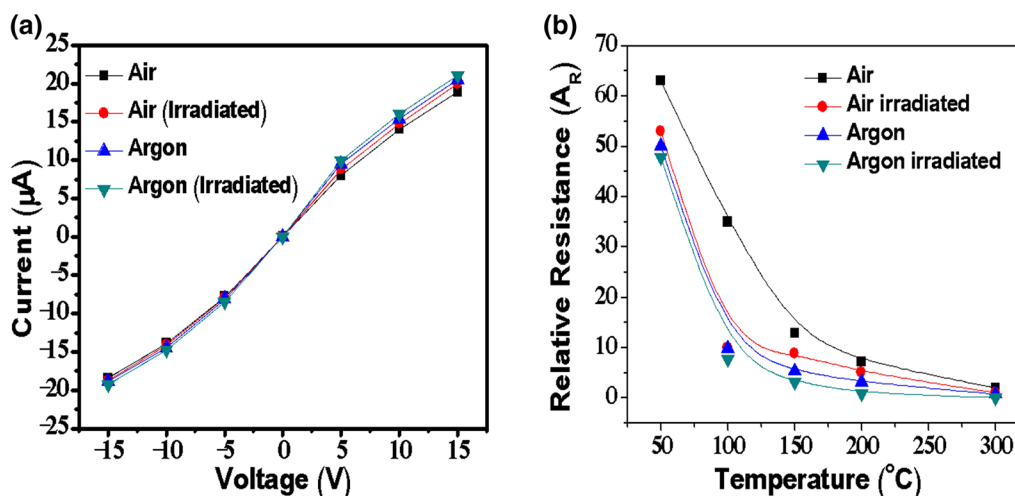


Fig. 7 Electrical characteristics of synthesized ZnO films showing the I – V curves of ZnO thin films annealed in non-inert and inert conditions; (b) ZnO thin film sensitivity towards temperature.

Photocatalytic Activity

Figure 9a shows a schematic of the photocatalytic degradation of MB using ZnO. Under UV illumination,

electron–hole pairs are generated (Eq. 8). Moreover, valence band (VB) electrons are transferred to the conduction band (CB), leaving an equal number of holes in the VB. Holes in the VB interact with surface water and generate OH[•] (Eq. 9).

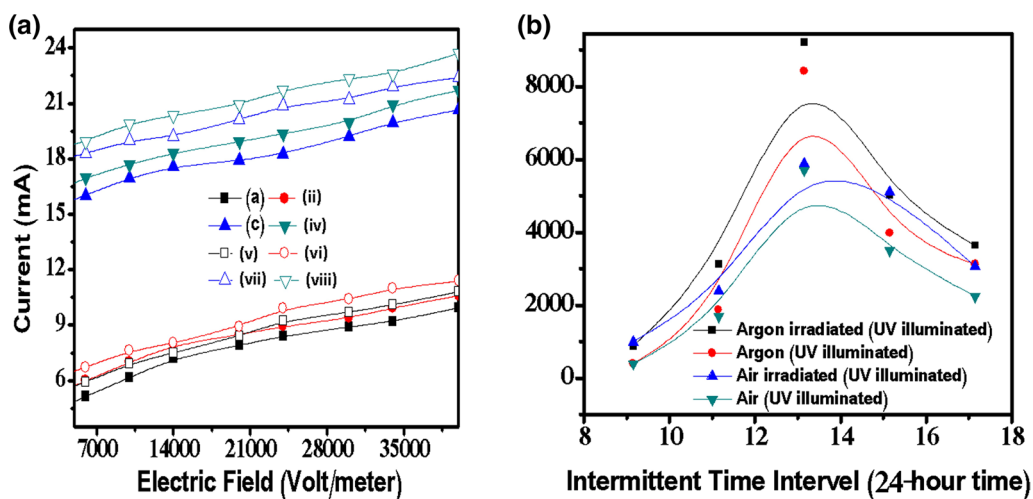


Fig. 8 Photoconductivity studies of ZnO thin films. (a) Photoresponse of the ZnO films under UV illumination: (i) the dark current of the sample annealed in air condition (unirradiated), (ii) photocurrent of the sample annealed in air (unirradiated), (iii) dark current of the sample annealed in the air (irradiated), (iv) photocurrent of the sample annealed in the air (irradiated), (v) dark current of the sample annealed in inert condition (unirradiated), (vi) photocurrent of the

sample annealed in argon atmosphere (unirradiated), (vii) dark current of sample annealed in argon atmosphere (irradiated), (viii) photocurrent of the sample annealed in argon atmosphere (irradiated). (b) Effect of electron beam irradiation and UV exposure on the relative resistance of synthesized ZnO films annealed in air and argon atmospheres.

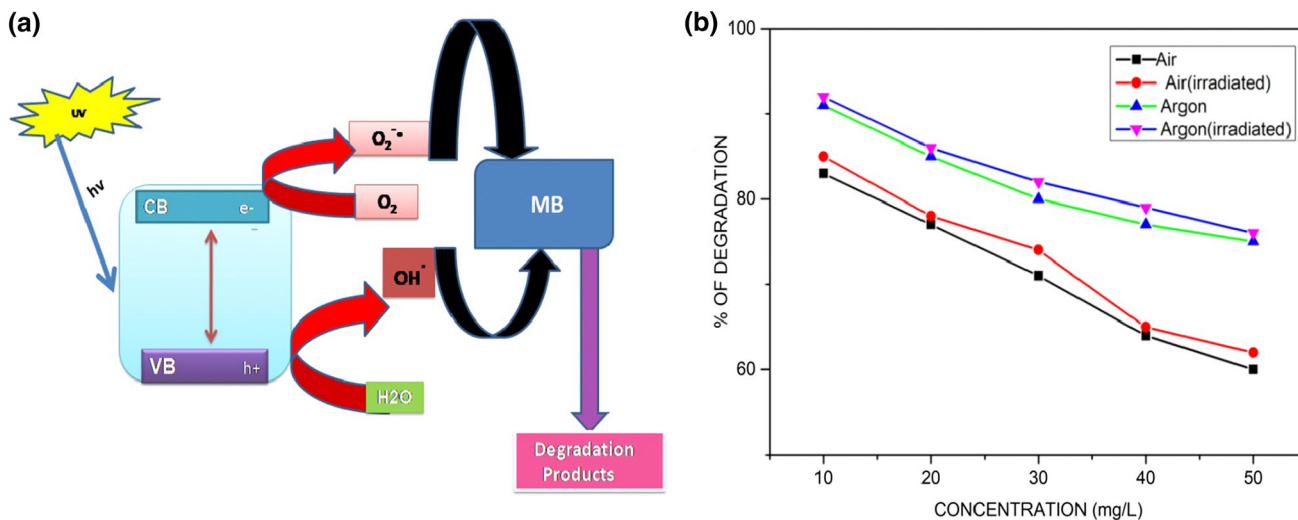


Fig. 9 Photodegradation of MB by ZnO: (a) schematic of the mechanism of photocatalytic degradation of MB using ZnO, (b) effect of initial concentration of MB on degradation at 25°C after 60 min.

The electrons excited to the CB generate superoxide anion (O_2^-) combining with surface O_2 . The unstable O_2^- radical eventually decomposes to OH^\cdot (Eq. 10). The generated OH^\cdot free radicals degrade out of the MB through several steps, and finally CO_2 and H_2O are produced as end products (Eq. 11).

$$ZnO + hv \rightarrow ZnO(h_{VB}^+ + e_{CB}^-) \tag{8}$$

$$h_{VB}^+ + H_2O \rightarrow H^+ + OH^\cdot \tag{9}$$

$$e_{CB}^- + O_2 \rightarrow O_2^- + H_2O \rightarrow HO^{\cdot 2} \rightarrow H_2O_2 \rightarrow OH^- + OH^\cdot \tag{10}$$

$$MB + OH^\cdot \rightarrow CO_2 + H_2O \tag{11}$$

Figure 9b shows the photocatalytic activities of synthesized ZnO films (with and without irradiation) under UV

illumination, evaluated by the photodegradation of MB dye. For systematic analysis of the ZnO photocatalytic ability, the photodegradation of MB was studied for different concentrations varying from 10 mg/L to 50 mg/L at 25°C, and under a UV exposure for 60 min. From Fig. 9b, it can be observed that, as the concentration of MB dye increases from 10 mg/L to 50 mg/L, the degradation efficiency of all the ZnO films decreases significantly. The pollutants are mainly degraded either by reaction with generated intermediate oxygen species or via direct oxidation by photogenerated holes. Thus, under a fixed UV illumination intensity, the photogenerated electron–hole pairs and number of hydroxyl radicals generated on the ZnO surface remain almost constant. As a result, the number of hydroxyl radicals required for photodegradation of the MB solutions with higher concentrations will not be sufficient, and the photodegradation efficiency decreases with an increase in dye concentration. From Fig. 9b, it can be observed that, irrespective of the MB dye concentration, the ZnO film annealed in an inert atmosphere shows enhanced photocatalytic efficiency compared to the air-annealed ZnO film. From the literature, it is well known that the separation efficiency of photogenerated electron–hole pairs is the key factor in photocatalytic activity. From the XRD analysis (see Fig. 3b), it is evident that a ZnO film annealed in inert conditions has an improved crystalline structure compared to air-annealed film. Moreover, the improved crystallinity suggests the decrease of the deep level defects in argon-annealed ZnO film. Deep level defects induce new energy levels within the band gap which act as the charge recombination centers, and in turn decrease the photocatalytic activity of the ZnO.⁶² Thus, argon-annealed ZnO film

exhibits improved photogenerated charge separation, and a decrease in deep level defects assists in enhanced charge transfer efficiency compared to air-annealed ZnO film. As a result, irrespective of the MB concentration, the photocatalytic efficiency of the inert condition-annealed film is better than air-annealed film. Further, the photodegradation of MB was analyzed after irradiating ZnO films with an electron beam. The results of the photo-degradation study reveal that the photocatalytic activity of the ZnO_{air} and ZnO_{argon} films irradiated with electrons is higher compared to their respective virgin films (see Fig. 9b). The electron irradiation induced surface defects and surface roughness in ZnO film.⁶³ In general, surface defects can serve as active sites, which are favorable for photocatalytic activity. Thus, the observed higher rate of degradation by electron-irradiated ZnO films can be attributed to the increase in surface defects as well as to the increased surface area. The best photocatalytic performance was exhibited by the ZnO film annealed in an inert atmosphere and irradiated with an electron beam. The sample exhibited a degrading efficiency of 90% for 10mg/L MB concentration. This enhanced photocatalytic activity is ascribed to the reduction of the deep level defects by annealing in an inert atmosphere and increasing the surface activity by irradiating with an electron beam.

All the samples displayed the highest photocatalytic activity for a low concentration of MB dye. Thus, a time-dependent photodegradation efficiency of all the samples was studied for the 10 mg/L concentration of MB dye. Figure 10a shows the influence of time on the photocatalytic degradation of the MB solution (10 mg/L) at 25°C by different ZnO films. Maximum degradation was observed at

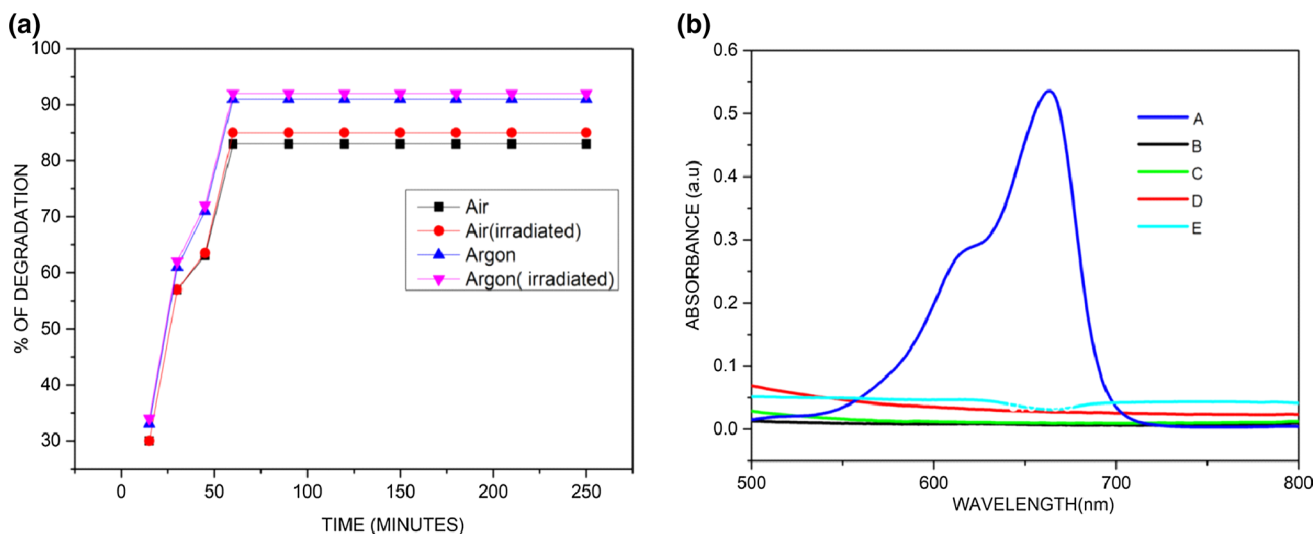


Fig. 10 Time-dependent photodegradation scheme for MB by ZnO film: (a) effect of contact time on the degradation of MB solution (10mg/L) at 25°C. (b) Absorption spectra of MB dye solution before and after photodegradation by various ZnO films: curve A represents

a MB solution before degradation and curves B, C, D, and E represent the extent to which MB was degraded by ZnO films, air, air-irradiated, argon, and argon-irradiated, respectively.

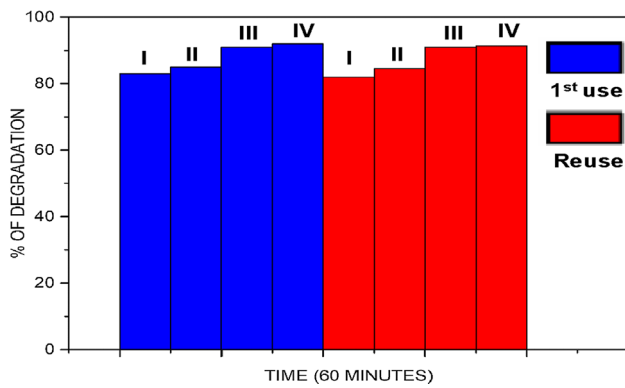


Fig. 11 Efficiency comparison of ZnO films catalysts and reused catalysts: *I* air, *II* air-irradiated, *III* argon, *IV* argon-irradiated.

60 min, and thereafter remained constant. For ZnO films, air, air irradiated, argon, and argon-irradiated, the maximum degradation efficiencies of the MB dye were 83%, 85%, 91%, and 92%, respectively. Furthermore, to analyze the photodegradation of the MB dye, the photodegraded solution was monitored at intervals of 30 min by UV-Vis absorbance spectra. Figure 10b shows the absorption spectra of MB dye solution before and after photodegradation by various ZnO films. The dye shows an absorption maximum at 619 nm before treatment, but no such absorption peak was noticed after photodegradation. The existence of the peak at 619 nm confirms the photodegradation of the MB dye by various ZnO films.

The reusability of the catalyst is one of the important aspects to be considered while performing photocatalytic studies. The stability of the catalyst over time and ease of recycling are the key criteria for evaluating the reusability of the catalyst. Figure 11 shows the comparison of the photodegradation efficiencies of fresh and reused ZnO films. The ZnO films used were washed and dried after usage and the catalytic studies were repeated. The photodegradation efficiencies of ZnO films after the 2nd cycle of MB dye (10 mg/L) degradation were compared with those of the fresh ZnO films, air, air-irradiated, argon, argon-irradiated. The reused samples show almost similar photodegradation efficiency as that of fresh ZnO films.

Table I represents the comparison of various ZnO films studied in terms of photocatalytic activity. From the table, it can be inferred that the present ZnO film exhibits comparable efficiency even for a high concentration of the MB dye (10 mg/L). Thus, the synthesized ZnO film can be employed as a catalyst with efficient reusability.

Conclusions

The present work examined the sensing properties of ZnO thin films synthesized via the mSILAR method under different experimental conditions printed on an FR-4 sheet. The comparative study of electrical properties, photoresponse, and photocatalytic activity of air/inert conditions-annealed and high energy beam-irradiated ZnO film was carried out. The electron beam-radiated sample (inert atmosphere) exhibited better conductivity, photoresponse, and photocatalytic activity compared to the other samples. The photocatalytic performance of the films and their reusability were tested by the photodegradation of MB dye. It was evaluated that the optical, electrical properties, and sensitivity can be tuned through optimized experimental conditions and electron beam irradiation. The synthesized and optimized ZnO films could be utilized as a photosensor, a temperature sensor, and as an efficient photocatalyst. Thus, synthesized ZnO thin films can find applications in space-related systems, solar cells, flexible electronics, robotic devices and systems, optoelectronics, as well as in different industrial applications.

Acknowledgments This work was supported by the NPRP Grant #NPRP11S-1221-170116 from the Qatar National Research Fund (a member of Qatar Foundation). The statements made herein are solely the responsibility of the authors.

Data availability The raw/processed data required to reproduce these findings cannot be shared at this time as the data also forms part of an ongoing study.

Conflict of interest On behalf of all authors, the corresponding author states that there is no conflict of interest.

Table I Photocatalytic activity comparison of various ZnO films reported in the literature.

Catalyst	Preparation method	Light source and contact time	Concentration of dye solution (mg/L)	% of degradation	References
ZnO thin film	Sol gel spin coating method	UV light, 240 min	5	90.4	64
ZnO thin film	Sol-gel dip-coating technique	Black light illumination, 300 min	5	70.34	65
ZnO thin film	Electron beam evaporation	UV light, 240 min	5	100	66
ZnO thin film	mSILAR	UV light, 60 min	10	92	Present work

References

- X. Xue, H. Chen, Y. Xiong, R. Chen, M. Jiang, G. Fu, Z. Xi, X.L. Zhang, J. Ma, W. Fang, and Z. Jin, Near-Infrared-Responsive Photo-Driven Nitrogen Fixation Enabled by Oxygen Vacancies and Sulfur Doping in Black $\text{TiO}_{2-x}\text{S}_y$ Nanoplatelets. *ACS Appl. Mater. Interfaces* 13, 4975 (2021). <https://doi.org/10.1021/acsami.0c17947>.
- W. Zhang, Y. Hu, C. Yan, D. Hong, R. Chen, X. Xue, S. Yang, Y. Tian, Z. Tie, and Z. Jin, Surface Plasmon Resonance Enhanced Direct Z-Scheme $\text{TiO}_2/\text{ZnTe}/\text{Au}$ Nanocorn Cob Heterojunctions for Efficient Photocatalytic Overall Water Splitting. *Nanoscale* 11, 9053 (2019). <https://doi.org/10.1039/c9nr01732a>.
- X. Xue, R. Chen, H. Chen, Y. Xu, Q. Ding, Z. Liu, L. Ma, G. Zhu, W. Zhang, Q. Yu, J. Liu, J. Ma, and Z. Jin, Oxygen Vacancy Engineering Promoted Photocatalytic Ammonia Synthesis on Ultrathin Two-Dimensional Bismuth Oxybromide Nanosheets. *Nano Lett.* 18, 7372 (2018). <https://doi.org/10.1021/acs.nanolett.8b03655>.
- X. Wang, X. Li, Q. Zhang, Z. Lu, H. Song, and Y. Wang, Electrodeposition of ZnO Nanorods with Synergistic Photocatalytic and Self-Cleaning Effects. *J. Electron. Mater.* 50, 4954 (2021). <https://doi.org/10.1007/s11664-021-08958-w>.
- A. Wojcik, M. Godlewski, E. Guzewicz, R. Minikayev, and W. Paszkowicz, Controlling of Preferential Growth Mode of ZnO Thin Films Grown by Atomic Layer Deposition. *J. Cryst. Growth* 310, 284 (2008). <https://doi.org/10.1016/j.jcrysgro.2007.10.010>.
- M.C. Sneed and R.C. Brasted, *Comprehensive Inorganic Chemistry*, Vol. 4 (New York: Princeton University Press, 1955).
- S. Goutham, S. Kaur, K.K. Sadasivuni, J.K. Bal, N. Jayarambabu, D.S. Kumar, and K.V. Rao, Nanostructured ZnO Gas Sensors Obtained by Green Method and Combustion Technique. *Mater. Sci. Semicond. Process.* 57, 110 (2017). <https://doi.org/10.1016/j.mssp.2016.09.037>.
- S. Mondal, K.P. Kanta, and P. Mitra, Preparation of ZnO Film on p-Si and I-V Characteristics of p-Si/n-ZnO. *Mat. Res.* 16, 94 (2013). <https://doi.org/10.1590/S1516-14392012005000149>.
- C.S. Prajapati and P.P. Sahay, Growth, Structure and Optical Characterization of Al-Doped ZnO Nanoparticle Thin Films. *Cryst. Res. Technol.* 46, 1086 (2011). <https://doi.org/10.1002/crat.201100192>.
- D. Thomas, S. Augustine, K.K. Sadasivuni, D. Ponnamma, A.Y. Alhaddad, J.J. Cabibihan, and K.A. Vijayalakshmi, Microtron Irradiation Induced Tuning of Band Gap and Photoresponse of Al-ZnO Thin Films Synthesized by mSILAR. *J. Electron. Mater.* 45, 4847 (2016). <https://doi.org/10.1007/s11664-016-4673-4>.
- N. Rabie, M. Bagherzadeh, M. Kiani, A.M. Ghadiri, K. Zhang, Z. Jin, S. Ramakrishna, and M. Shokouhimehr, High Gravity-Assisted Green Synthesis of ZnO Nanoparticles via *Allium ursinum*: Conjoining Nanochemistry to Neuroscience. *Nano Exp.* 1, 020025 (2020). <https://doi.org/10.1088/2632-959X/abac4d>.
- G. Xiangdong, L. Xiaomin, and Y. Weidong, Preparation and Characterization of Highly Oriented ZnO Film by Ultrasonic Assisted SILAR Method. *J. Wuhan Univ. Technol. Mater. Sci. Ed.* 20, 23 (2005). <https://doi.org/10.1007/BF02835019>.
- D. Fang, C. Li, N. Wang, P. Li, and P. Yao, Structural and Optical Properties of Mg-Doped ZnO Thin Films Prepared by a Modified Pechini Method. *Cryst. Res. Technol.* 48, 265 (2013). <https://doi.org/10.1002/crat.201200437>.
- V. Shelke, B. Sonawane, M. Bhole, and D. Patil, Electrical and Optical Properties of Transparent Conducting Tin Doped ZnO Thin Films. *J. Mater. Sci. Mater. Electron.* 23, 451 (2012). <https://doi.org/10.1007/s10854-011-0462-2>.
- T. Yen, D. Strome, S.J. Kim, A. Cartwright, and W.A. Anderson, Annealing Studies on Zinc Oxide Thin Films Deposited by Magnetron Sputtering. *J. Electron. Mater.* 37, 764 (2008). <https://doi.org/10.1007/s11664-007-0357-4>.
- M.R. Maurya and V. Toutam, Fast Response UV Detection Based on Waveguide Characteristics of Vertically Grown ZnO Nanorods Partially Embedded in Anodic Alumina Template. *Nanotechnology* 30, 085704 (2018). <https://doi.org/10.1088/1361-6528/aaf545>.
- M.R. Maurya, V. Toutam, S. Bathula, P. Pal, and B.K. Gupta, Wide Spectral Photoresponse of Template Assisted Out of Plane Grown ZnO/NiO Composite Nanowire Photodetector. *Nanotechnology* 31, 025705 (2019). <https://doi.org/10.1088/1361-6528/ab474e>.
- J. Son, J. Shim, and N. Cho, Variations in Electrical and Physical Properties of Al:ZnO Films with Preparation Conditions. *Met. Mater. Int.* 17, 99 (2011). <https://doi.org/10.1007/s12540-011-0213-1>.
- P. Murmu, J. Kennedy, B. Ruck, G. Williams, A. Markwitz, S. Rubanov, and A. Suvorova, Effect of Annealing on the Structural, Electrical and Magnetic Properties of Gd-Implanted ZnO Thin Films. *J. Mater. Sci.* 47, 1119 (2012). <https://doi.org/10.1007/s10853-011-5883-z>.
- H. Zhu, J. Hpkas, E. Bunte, A. Gerber, and S. Huang, Influence of Working Pressure on ZnO: Al Films from Tube Targets for Silicon Thin Film Solar Cells. *Thin Solid Films* 518, 4997 (2012). <https://doi.org/10.1016/j.tsf.2010.02.065>.
- W.H. Luo, T.K. Tsai, J.C. Yang, W.M. Hsieh, C.H. Hsu, and J.S. Fang, Enhancement in Conductivity and Transmittance of Zinc Oxide Prepared by Chemical Bath Deposition. *J. Electron. Mater.* 38, 2264 (2009). <https://doi.org/10.1007/s11664-009-0900-6>.
- Y. Kokubun, H. Kimura, and S. Nakagomi, Preparation of ZnO Thin Films on Sapphire Substrates by Sol-Gel Method. *Jpn. J. Appl. Phys.* 42, L904 (2003). <https://doi.org/10.1143/JJAP.42.L904>.
- A. Ennaqoui, M. Weber, R. Scheer, and H.J. Lewerenz, Chemical-Bath ZnO Buffer Layer for CuInS_2 Thin-Film Solar Cells. *Sol. Energy Mater. Sol. Sol.* 54, 277 (1998). [https://doi.org/10.1016/S0927-0248\(98\)00079-8](https://doi.org/10.1016/S0927-0248(98)00079-8).
- M.R. Maurya, V. Toutam, and D. Haranath, Comparative Study of Photoresponse from Vertically Grown ZnO Nanorod and Nanoflake Films. *ACS Omega* 2, 5538 (2017). <https://doi.org/10.1021/acsomega.7b00914>.
- S. Ilican, Y. Caglar, and M. Caglar, Preparation and Characterization of ZnO Thin Films Deposited by Sol-Gel Spin Coating Method. *J. Optoelectron Adv. Mater.* 10, 2578 (2008).
- W. Tang and D.C. Cameron, Aluminum-Doped Zinc Oxide Transparent Conductors Deposited by the Sol-Gel Process. *Thin Solid Films* 238, 83 (1994). [https://doi.org/10.1016/0040-6090\(94\)90653-X](https://doi.org/10.1016/0040-6090(94)90653-X).
- Y. Natsume and H. Sakata, Zinc Oxide Films Prepared by Sol-Gel Spin-Coating. *Thin Solid Film.* 372, 30 (2000). [https://doi.org/10.1016/S0040-6090\(00\)01056-7](https://doi.org/10.1016/S0040-6090(00)01056-7).
- T. Ivanova, A. Harizanova, T. Koutzarova, and B. Vertruyen, Study of ZnO Solgel Films: Study of ZnO Solgel Films: Effect of Annealing". *Mater. Lett.* 64, 1147 (2010). <https://doi.org/10.1016/j.matlet.2010.02.033>.
- Z.R. Khan, M.S. Khan, M. Zulfequar, and M.S. Khan, Optical and Structural Properties of ZnO Thin Films Fabricated by Sol-Gel Method. *Mater. Sci. Appl.* 2, 340 (2011).
- M.N. Kamalasanan and S. Chandra, Sol-Gel Synthesis of ZnO Thin Films. *Thin Solid Films* 288, 112 (1996). <https://doi.org/10.4236/msa.2011.25044>.
- A. Pakdel and F.E. Ghodsi, Influence of Drying Conditions on the Optical and Structural Properties of Sol-Gel Derived ZnO Nanocrystalline films. *Pramana J. Phys.* 76, 973 (2011).

32. Y. Zhou, P.J. Kelly, A. Postill, O.A. Zeid, and A.A. Almajjar, The Characteristics of Aluminium-Doped Zinc Oxide Films Prepared by Pulsed Magnetron Sputtering from Powder Targets. *Thin Solid Films* 447–448, 33 (2004). <https://doi.org/10.1016/j.tsf.2003.09.018>.
33. E.G. Fu, D.M. Zhang, G. Zhang, Z. Ming, Z.F. Yang, and J.J. Liu, Properties of Transparent Conductive ZnO: Al Thin Films Prepared by Magnetron Sputtering. *Microelectron. J.* 35, 383 (2004). [https://doi.org/10.1016/S0026-2692\(03\)00251-9](https://doi.org/10.1016/S0026-2692(03)00251-9).
34. E.M. Kaidashev, M. Lorenz, H.V. Wenckstern, A. Rahm, H.C. Semmelhack, K.H. Han, G. Benndorf, C. Bundesmann, H. Hochmuth, and M. Grundmann, High Electron Mobility of Epitaxial ZnO Thin Films on c-Plane Sapphire Grown by Multistep Pulsed-Laser Deposition. *Appl. Phys. Lett.* 82, 3901 (2003). <https://doi.org/10.1063/1.1578694>.
35. V. Craciun, J. Elders, J.G.E. Gardeniers, and I.W. Boyd, Characteristics of High Quality ZnO Thin Films Deposited by Pulsed Laser Deposition. *Appl. Phys. Lett.* 65, 2963 (1994). <https://doi.org/10.1063/1.112478>.
36. V. Srikant, V. Sergo, and D.R. Clarke, Epitaxial Aluminum-Doped Zinc Oxide Thin Films on Sapphire: I, Effect of Substrate Orientation. *J. Am. Ceram. Soc.* 78, 1931 (1995). <https://doi.org/10.1111/j.1151-2916.1995.tb08912.x>.
37. S.L. King, J.G.E. Gardeniers, and I.W. Boyd, Pulsed-Laser Deposited ZnO for Device Applications. *Appl. Surf. Sci.* 96, 811 (1996). [https://doi.org/10.1016/0169-4332\(96\)80027-4](https://doi.org/10.1016/0169-4332(96)80027-4).
38. B. Ghosh, H. Dutta, and S.K. Pradhan, Microstructure Characterization of Nanocrystalline Ni₃C Synthesized by High Energy Ball Milling. *J. Alloys Compd.* 479, 193 (2009). <https://doi.org/10.1016/j.jallcom.2008.12.133>.
39. O. Pagni, N.N. Somhlahlhlo, C. Weichsel, and A.W.R. Leitch, Electrical Properties of ZnO Thin Films Grown by MOCVD. *Phys. B Condens. Matter* 376, 749 (2006). <https://doi.org/10.1016/j.physb.2005.12.187>.
40. L. Changqing, J. Zhong, C. Haibin, and L. Yan, Seed-Mediated Growth of ZnO Nanorods on Multiwalled Carbon Nanotubes. *J. Nanosci. Nanotechnol.* 8, 4441 (2008). <https://doi.org/10.1166/jnn.2008.278>.
41. K. Saito, Y. Watanabe, K. Takahashi, T. Matsuzawa, B. Sang, and M. Konagai, Photo Atomic Layer Deposition of Transparent Conductive ZnO Films. *Sol. Energy Mater Sol.* 49, 187 (1997). [https://doi.org/10.1016/S0927-0248\(97\)00194-3](https://doi.org/10.1016/S0927-0248(97)00194-3).
42. M. Kasuga and M. Mochizuki, Orientation Relationships of Zinc Oxide on Sapphire in Heteroepitaxial Chemical Vapor Deposition. *J. Cryst. Growth* 54, 185 (1981). [https://doi.org/10.1016/0022-0248\(81\)90459-0](https://doi.org/10.1016/0022-0248(81)90459-0).
43. S.K. Ghandi, R.J. Field, and J.R. Shealy, Highly Oriented Zinc Oxide Films Grown by the Oxidation of Diethylzinc. *Appl. Phys. Lett.* 37, 449 (1980). <https://doi.org/10.1063/1.91960>.
44. T.M. Barnes, J. Leaf, C. Fry, and C.A. Wolden, Room temperature Chemical Vapor Deposition of c-Axis ZnO. *J. Cryst. Growth* 274, 412 (2005). <https://doi.org/10.1016/j.jcrysgro.2004.10.015>.
45. A. Jiménez-González and R. Suarez-Parra, Effect of Heat Treatment on the Properties of ZnO Thin Films Prepared by Successive Ion Layer Adsorption and Reaction (SILAR). *J. Cryst. Growth* 167, 649 (1996). [https://doi.org/10.1016/0022-0248\(96\)00308-9](https://doi.org/10.1016/0022-0248(96)00308-9).
46. S.S. Kale, R.S. Mane, H.M. Pathan, A.V. Shaikh, O.S. Joo, and S.H. Han, Preparation and Characterization of ZnTe Thin Films by SILAR Method. *Appl. Surf. Sci.* 253, 4335 (2007). <https://doi.org/10.1016/j.apsusc.2006.09.043>.
47. S. Mondal, S.R. Bhattacharyya, and P. Mitra, Preparation of Manganese-Doped ZnO Thin Films and Their Characterization. *Bull Mater Sci* 36, 223 (2013). <https://doi.org/10.1007/s12034-013-0462-3>.
48. J.H. Lee and B.O. Park, Characteristics of Al-Doped ZnO Thin Films Obtained by Ultrasonic Spray Pyrolysis: Effects of Al Doping and an Annealing Treatment. *Mater. Sci. Eng. B* 106, 242 (2004). <https://doi.org/10.1016/j.mseb.2003.09.040>.
49. T.Y. Ma and S.C. Lee, Effects of Aluminum Content and Substrate Temperature on the Structural and Electrical Properties of Aluminum-Doped ZnO Films Prepared by Ultrasonic Spray Pyrolysis. *J. Mater. Sci. Mater. Electron.* 11, 305 (2000). <https://doi.org/10.1023/A:1008925315123>.
50. C. Agashe, M.G. Takawale, B.R. Marathe, and V.G. Bhide, Structural Properties of SnO₂: F Films Deposited by Spray Pyrolysis. *Sol. Energy Mater.* 17, 99 (1998). [https://doi.org/10.1016/0165-1633\(88\)90010-X](https://doi.org/10.1016/0165-1633(88)90010-X).
51. Y.F. Nicolau and J.C. Menard, Solution Growth of ZnS, CdS and Zn_{1-x}Cd_xS Thin Films by the Successive Ionic-Layer Adsorption and Reaction Process; Growth Mechanism. *J. Cryst. Growth* 92, 128 (1998). [https://doi.org/10.1016/0022-0248\(88\)90443-5](https://doi.org/10.1016/0022-0248(88)90443-5).
52. M. Ristov, G.J. Sinadinovski, I. Grozdanov, and M. Mitreski, Chemical Deposition of ZnO Films. *Thin Solid Films* 149, 65 (1987). [https://doi.org/10.1016/0040-6090\(87\)90249-5](https://doi.org/10.1016/0040-6090(87)90249-5).
53. A.E. Rakhshani, Al-Doped Zinc Oxide Films Grown by Successive Chemical Solution Deposition. *Appl. Phys. A* 92, 413 (2008). <https://doi.org/10.1007/s00339-008-4542-y>.
54. A.E. Jimenez-Gonzalez and P.K. Nair, Photosensitive ZnO Thin Films Prepared by the Chemical Deposition Method SILAR. *Semicond. Sci. Technol.* 10, 1277 (1995). <https://doi.org/10.1088/0268-1242/10/9/013>.
55. P. Mitra and J. Khan, Chemical Deposition ZnO Films From Ammonium Zincateath. *Mater. Chem. Phys.* 98, 279 (2006). <https://doi.org/10.1016/j.matchemphys.2005.09.042>.
56. S. Mondal and P. Mitra, Preparation of Cadmium Doped ZnO Thin Films by SILAR and Their Characterization. *Bull. Mater. Sci.* 5, 751 (2012). <https://doi.org/10.1007/s12034-012-0350-2>.
57. M. Jung, J. Lee, S. Park, H. Kim, and J. Chang, Investigation of the Annealing Effects on the Structural and Optical Properties of Sputtered ZnO Thin Films. *J. Cryst. Growth.* 283, 384 (2005). <https://doi.org/10.1016/j.jcrysgro.2005.06.047>.
58. T. Ungar and A. Borbely, The Effect of Dislocation Contrast on X-Ray Line Broadening: A New Approach to Line Profile Analysis. *Appl. Phys. Lett.* 69, 3173 (2009). <https://doi.org/10.1063/1.117951>.
59. N. Choudhury and B.K. Sarma, Structural Characterization of Lead Sulfide Thin Films by Means of X-Ray Line Profile Analysis. *Bull. Mat. Sci.* 32, 43 (2009). <https://doi.org/10.1007/s12034-009-0007-y>.
60. H.P. Klug and L.E. Alexander, *X-Ray Diffraction Procedures for Polycrystalline and Amorphous Materials*, 2nd ed., (New York: Wiley, 1974).
61. K.K. Sadasivuni, A. Kafy, H.C. Kim, H.U. Ko, S. Mun, and J. Kim, Reduced Graphene Oxide Filled Cellulose Films for Flexible Temperature Sensor Application. *Synth. Met.* 206, 154 (2015). <https://doi.org/10.1016/j.synthmet.2015.05.018>.
62. D. Chen, Z. Wang, T. Ren, H. Ding, W. Yao, R. Zong, and Y. Zhu, Influence of Defects on the Photocatalytic Activity of ZnO. *J. Phys. Chem.* 118, 15300 (2014). <https://doi.org/10.1021/jp5033349>.
63. K.B. Sapnar, L.A. Ghule, S.V. Bhoraskar, K.M. Garadkar, S.D. Dhole, and V.N. Bhoraskar, Photocatalytic Activity of 65 MeV Electron-Irradiated ZnO Nanorods. *Radiat. Effects Defects Solids* 167, 238 (2012). <https://doi.org/10.1080/10420150.2011.614613>.
64. S. Shankar, M. Saroja, M. Venkatachalam, and G. Parthasarathy, Photocatalytic Degradation of Methylene Blue Dye Using ZnO Thin Films. *Int. J. Chem. Concepts* 3, 180 (2017).
65. P. Jongnavakit, P. Amornpitoksuk, S. Suwanboon, and T. Ratana, Surface and Photocatalytic Properties of ZnO Thin Film Prepared by Sol–Gel Method. *Thin Solid Films* 520, 5561 (2012). <https://doi.org/10.1016/j.tsf.2012.04.050>.

66. N. Talebian and M.R. Nilforoushan, Comparative Study of the Structural, Optical and Photocatalytic Properties of Semiconductor Metal Oxides Toward Degradation of Methylene Blue. *Thin Solid Films* 518, 2210 (2010). <https://doi.org/10.1016/j.tsf.2009.07.135>.

Publisher's Note Springer Nature remains neutral with regard to jurisdictional claims in published maps and institutional affiliations.